Active communities and growth of soil microorganisms are framed by mean annual precipitation in three California annual grasslands

Megan M. Foley[1,2], Steven J. Blazewicz[3], Karis J. McFarlane[3], Alex Greenlon[4], Michaela Hayer[1,2], Jeffrey A. Kimbrel[3], Benjamin J. Koch[1,2], Keith Morrison[3], Ember Morrissey[5], Bruce A. Hungate[1,2], Jennifer Pett-Ridge[3,6]

1. Center for Ecosystem Science and Society, Northern Arizona University, Flagstaff AZ, USA
2. Department of Biological Sciences, Northern Arizona University, Flagstaff AZ, USA
3. Physical and Life Sciences Directorate, Lawrence Livermore National Laboratory, Livermore, CA, USA
4. Department of Environmental Science, Policy, and Management, University of California, Berkeley CA, USA
5. Division of Plant and Soil Sciences, West Virginia University, Morgantown, West Virginia, USA
6. Life & Environmental Sciences Department, University of California Merced, Merced, California, USA

Abstract

Earth system models project altered precipitation regimes across much of the globe. In California, the winter wet season is predicted to extend into spring, and the summer dry period to lengthen. How altered precipitation will affect soil carbon (C) persistence is a key knowledge gap. However, we do not have a mechanistic understanding of how altered soil moisture regimes will affect microbial population dynamics. Using quantitative stable isotope probing (qSIP), we compared total and active soil microbial communities across three California annual grassland ecosystems that span a rainfall gradient and have developed upon similar parent material. We also assessed multiple edaphic variables, including available C and the radiocarbon (^{14}C) age of soil C. Samples were assayed in the wet season, when we expected environmental conditions would be most similar across sites. We hypothesized that the long-term legacy of soil water limitation would be reflected in lower community growth capacity at the driest site. We also predicted that actively growing communities would be more compositionally similar across the gradient than the total background microbiome. Across the three sites, edaphic parameters such as pH roughly sorted with mean annual precipitation, and soil carbon age increased with precipitation. Bacterial growth rates increased from the driest site to the intermediate site, and rates were comparable between the intermediate and wettest sites. These differences were persistent across major phyla, including the Actinobacteria, Bacteroidetes, and Proteobacteria. Taxonomic identity was a strong predictor of growth, such that the growth rates of a taxon at one site predicted its growth rates at the others. We think this fact, that taxa that grew quickly at one site tended to grow quickly at the others, is likely a consequence of genetically determined physiological traits, and is consistent with the idea that evolutionary history influences growth rate.

Introduction

Rainfall patterns and soil water content are ultimate controllers of microbial population dynamics (growth and death) and Earth system models project major changes in the timing and intensity of precipitation events globally[1,2]. Since microorganisms mediate a wide range of ecosystem processes, understanding how a site's climate history impacts microbial communities is essential. In Mediterranean climates, seasonal fluctuations between dry and wet seasons can drive dramatic changes in microbial community structure and function[3,4]. Microorganisms indigenous to these ecosystems must withstand both direct physiological stress during prolonged periods of low soil moisture and be able to compete for resources when seasonal rains return and plant growth resumes[5].

Historic exposure to low soil water potential can have a lasting effect on microbial respiration, enzyme activity, and carbon use efficiency[6–8], and is likely to influence growth as well. Repeated exposure to limited soil moisture may select for traits that confer tolerance to water stress and against traits that enhance organisms' ability to grow efficiently or acquire resources[9–11]. If so, soil microorganisms subject to prolonged moisture deficits may grow more slowly, because of ecophysiological adaptations that incur a cost to growth. For example, the production of extracellular polymeric substances can be a substantial carbon sink for bacteria growing under water stress while osmolyte regulation in response to water stress can consume both nutrients and energy[12,13]. If such traits are advantageous under chronic water stress, genomic and biochemical cost to maintain such systems may ensue. This, microbial taxa from soils exposed to chronic water stress might be expected to grow more slowly even in the absence of immediate water stress.

Soil water dynamics also shape the structure of microbial communities[14,15]. Most studies of soil microbial diversity rely on sequencing of total DNA, which typically includes genetic material from not only active cells, but also dead and dormant microorganisms. Growing, dormant, and dead microorganisms all play vital roles in soils, but those roles are distinct, so distinguishing among them is important. The inability to distinguish among dead, dormant, and growing microorganisms obscures ecological processes driving microbial community composition. For example, compared to the total community detected through DNA sequencing, active soil communities generally show a heightened sensitivity to changes in environmental conditions, and active microbes in dry ecosystems appear to be more strongly influenced by dynamic environmental conditions such as changes in soil water[16,17]. Alternatives, such as RNA-based approaches to distinguish between dormant and metabolically active microorganisms, have been criticized, and we still lack an understanding of the structure of microbial communities exclusive of dead and dormant organisms[18].

In our study, we compared total and active microbial communities and soil edaphic characteristics across three California annual grassland ecosystems with Mediterranean-type climates that span a rainfall gradient and developed upon similar parent material. First, we characterized the soils to understand how diverging water regimes have shaped the physiochemical environment that soil microbes experience within each ecosystem. We then quantitatively analyzed patterns of microbial population growth using quantitative stable isotope probing during the wet season, when soil water was not limiting. We hypothesized that growth would be slowest in the driest site even when differences in soil water content were minimized, reflecting the legacy cost of adaptation to limited soil moisture for microbial growth. Finally, we compare the structure of communities inferred from 16S rRNA sequencing (the "total

community") against the communities of growing organisms (the "growing community") at each site. We hypothesized that growing communities would be compositionally more similar to each other between sites than total communities, given the similarity in soil water content and plant phenology during the weeks immediately preceding our sampling.

Materials and Methods

Site description and sample collection

We characterized soil chemistry and bacterial and archaeal communities in three coastal California annual grasslands with Mediterranean-type climates. The sites span a significant rainfall gradient (388 mm yr^{-1} to 2833 mm yr^{-1}), yet have similar plant communities and soils developed on similar parent material (sedimentary rock and coastal terraces) (Table 1). The northmost site, Angelo Coast Range Reserve, lies upstream of the headwaters of the South Fork Eel River where indigenous peoples including the Cahto, Pomo, Wailaki, Yuki, Weott, and Sinkyone historically held territory[19]. Annual grasslands at Angelo intersperse mixed-oak woodland and old-growth conifer forest that occur on strath terraces which formed as the Eel River cut through the soft coastal sediment[20,21]. Hopland Research and Extension Center sits in the foothills of the Mayacamas Mountains about 96 km south of Angelo encompassing topographically rugged rangeland on territory originally occupied by the Pomo Nation. Furthest south, Sedgwick Reserve spans the Santa Ynez Valley and San Rafael Mountains and is located on land where the Chumash people have historically lived.

These sites developed on similarly-aged sedimentary rock of the Franciscan formation. At Angelo, parent materials are comprised of argillite and sandstone interbedding and soils are Ultic Haploxeralfs of the Hologan-Hollowtree-Casabonne complex[22]. At Hopland, soils

developed on weathered sandstone and shale, as well as metamorphic schist and are Typic Haploxeralfs of the Witherall-Squawrock complex[23]. Lastly, at Sedgwick, soils developed on ancient sandstone and shale, as well as alluvium from the Paso-Robles formation, and are Pachic Argixerolls belonging to the Botella series[24].

Naturalized non-native annual grasses dominate vegetation at the three sites. *Avena spp.* and *Bromus spp.* dominate at Hopland and Sedgwick[25,26]. Vegetation at Angelo is dominated by non-native annual grasses including *Aira caryophyllea, Bromus hordeaceuous,* and *Briza minor* and by annual and perennial forbs interspersed with the native perennial grass *Danthonia californica*[20,22,27] (Table 1). *Avena spp.* has also been observed at Angelo.

We collected soils in February-March 2018. At each site, surface vegetation was removed and three replicate soil cores (10 cm x 5 cm) were collected 1 m apart for chemical characterization, radiocarbon characterization, and quantitative stable isotope probing. Soil cores were transported on ice to Lawrence Livermore National Laboratory where they were homogenized by hand, stones and large roots were removed, and portions were dried at room temperature, stored at 4 °C, or frozen at -80 °C for different downstream analyses. All analyses reported here were conducted on surface soils (0-10 cm). We measured gravimetric soil water content by drying soils to a constant weight at 105°C. We retrieved daily mean air temperature and total precipitation data for the thirty-day period preceding sample collection at each site.

	Angelo Coast Range Reserve	**Hopland Research and Extension Center**	**Sedgwick Reserve**
Location	39°44.253`N, 123°37.823`W	39°00.106`N, 123°04.184`W	34°42.697'N, 120°2.333'W
Elevation (m)	475	180	360
MAT max/min (°C)	20/6	23/7	24/7

MAP (mm yr^{-1})	2160	956	383
Parent Material	Argillite/Sandstone interbedding	Sandstone, Shale, Graywacke, Schist	Alluvium, Calcareous shale, Acid sandstone
Soil Order	Alfisol	Alfisol	Mollisol
Soil Series	Holohand-Hollowtree-Casabonne complex	Witherell-Squawrock complex	Botella
Dominant vegetation	*Aira spp., Bromus spp., Briza spp.*	*Avena spp., Bromus spp., Erodium spp., Festuca spp.*	*Avena spp., Bromus spp.*

Table 1 Characteristics of the California annual grasslands examined in this study.

Soil physical and chemical characterization

Soil chemical and physical characterization was conducted at the Oregon State University Soil Health Laboratory. Bulk C and N concentrations were quantified by Elementar Vario Macro cube elemental analyzer through dry combustion, separation of gaseous species, and thermal conductivity detection. Trace elements were quantified by the Agilent 5110 ICP-OES after soils were extracted with 0.002M Barium chloride. Soil texture was determined by the hydrometer method. Soil pH was measured using a Mettler Toledo Seven Compact pH/Ion meter. To measure pH, 4 g of soil was suspended in 8 mL of 0.01 M $CaCl_2$ and equilibrated for 1 hour prior to analysis[28].

Additional soil cores were collected from the top 5 cm of soil from Sedgewick, Angelo and Buck field sites in June of 2019 for moisture analysis. Soil cores were also collected from the top 8-15 cm of soil to calculate bulk density. Intact soil cores were prepared and analyzed using Meter HYPROP in accordance with manufacturer's instructions. The HYPROP was used to generate a partial soil moisture release curve on wet soils. Additional cores were subsampled and analyzed using WP4C in accordance with manufacturer's instructions. The WP4C was used

to generate a partial soil moisture release curve on dry soils. Partial soil moisture release data generated by Hyprop and WP4C were used in accordance with manufacturer's instructions to generate complete soil moisture release curves using Hyprop fit software.

Quantitative X-ray diffraction

Quantitative X-ray diffraction (qXRD) was performed at the Space Science and Astrobiology Division at NASA's Ames Research Center. Samples for qXRD were crushed in a mortar and pestle and passed through a 250 µm sieve. The samples were spiked with 20 wt. % αAl_2O_3 (internal standard) and micronized for 5 minutes in ethanol using a McCrone mill. The ground samples were then transferred to a plastic tray and dried under heat lamps. The micronized samples sere then saturated with Vertrel® and vortexed with plastic beads to promote random orientation of the minerals. The random powders were side loaded into XRD sample mounts. All powdered samples were analyzed on a Rigaku Smartlab diffractometer using Cu k-alpha radiation and a scintillation detector with 1° divergence and receiving slits. The samples were scanned from 5° to 65° 2θ at 0.02° steps with a 2 second per step count time. Quantitative mineralogy was determined using the full pattern peak-fitting program RockJock 11[29].

Natural Abundance Stable Isotopes and Radiocarbon analysis of bulk soils and incubations

For each core, subsamples of dried homogenized soil were analyzed for $\delta^{13}C$ and $\delta^{15}N$ at the Center for Stable Isotope Biogeochemistry at the University of California, Berkeley (IsoPrime100 mass spectrometer) or prepared for bulk soil radiocarbon measurement by sealed-tube combustion to CO_2 in the presence of CuO and Ag. A subsample of fresh soil from each core was incubated in the lab to measure $\Delta^{14}CO_2$ of microbially respired carbon. Roots were

removed from soils by hand picking and left undisturbed for one week at room temperature to allow any remaining roots to senesce. For each core, approximately 150 g dry mass-equivalent soil was weighed into 150 mL beakers and placed inside quart-sized mason jars with stopcock-fitted lids. Soils were pre-incubated for one day before incubation jars were sealed and headspaces flushed with CO_2-free air. Soils were then incubated at room temperature until enough CO_2 had accumulated for ^{14}C measurement (9-11 days). At the end of the incubation period, headspace CO_2 was cryogenically purified for radiocarbon analysis. Aliquots of purified CO_2 were analyzed for $\delta^{13}C$ at the UC Davis Stable Isotope Laboratory (GVI Optima Stable Isotope Ratio Mass Spectrometer).

CO_2 from both combusted bulk soil and incubation jars was purified cryogenically at the Center for Accelerator Mass Spectrometry (CAMS) at Lawrence Livermore National Laboratory using a vacuum line before being reduced to graphite on iron powder in the presence of H_2 (Vogel et al., 1984). Radiocarbon abundance in graphitized samples was determined on the FN Van de Graaff Accelerator Mass Spectrometer at Lawrence Livermore National Laboratory's Center for Accelerator Mass Spectrometer. Radiocarbon values are reported in $\Delta^{14}C$ notation corrected for mass-dependent fractionation using measured $\delta^{13}C$ values[30].

^{18}O-water quantitative stable isotope probing (qSIP)

For SIP incubations, 5 g soil from each field replicate was transferred to 15 ml Nalgene flatbottom vials. Soils were dried in a laminar flow hood at room temperature for 24 hours prior to isotope addition. One milliliter of isotopically enriched water (98.15 at% ^{18}O-H_2O) or natural abundance water (as a control) was pipetted onto the soil slowly and evenly and gently mixed with the pipette tip. After the water addition, vials were immediately sealed inside 500 ml mason

jars and incubated at room temperature in the dark for 8 days. At the end of the incubation, soils were frozen in liquid nitrogen and then stored at -80°C.

DNA was extracted from all soil samples using a modified protocol adapted from Barnard (2015)[3]. Three replicate extractions were conducted for each sample and then replicate DNA extracts were combined. For each extraction, soil (0.4 g +/- 0.001) was added to 2 ml Lysing Matrix E tube (MP Biomedicals) and extracted twice as follows. 500 µl extraction buffer (5% CTAB, 0.5 M NaCl, 240 mM K_2HPO_4, pH 8.0) and 500 µl 25:24:1 phenol:chloroform:isoamyl alcohol were added before shaking (FastPrep24, MP Biomedicals: 30 s, 5.5 m $^{s-1}$). After centrifugation (16,100 x g, 5 min), residual phenol was removed using pre-spun 2 ml Phase Lock Gel tubes (5 Prime, Gaithersburg, MD, USA) with an equal volume of 24:1 chloroform:isoamyl alcohol, mixed and centrifuged (16,100 x g, 2 min). The aqueous phases from both extractions were pooled, mixed with 7 µl RNAase (10 mg/ml), mixed by inverting, and incubated at 50 °C for 10 min. 335 µL 7.5 M NH4+ acetate was added, mixed by inverting, incubated (4 °C, 1 h). and centrifuged (16,100 x g, 15 min. Supernatant was transferred to a new 1.7 ml tube and 1 µl Glycoblue (15 mg/ml) and 1 ml 40% PEG 6000 in 1.6 M NaCl were added, mixed by vortex, and incubated at room temperature in the dark (2 h). After centrifugation (16,100 x g, 20 min), the pellet was rinsed with 1 ml ice-cold 70% ethanol, air-dried, resuspended in 30 µl 1xTE and stored at -80 °C.

Samples were subjected to a cesium chloride density gradient formed by physical density separation via ultracentrifugation as previously described with minor modifications[31,32]. For each sample, 5 µg of DNA in 150 µL 1xTE was mixed with 1.00 mL gradient buffer, and 4.60 mL CsCl stock (1.885 g mL^{-1}) with a final average density of 1.730 g mL^{-1}. Samples were loaded into 5.2 mL ultracentrifuge tubes and spun at 20 ºC for 108 hours at 176,284 RCF_{avg} in a

Beckman Coulter Optima XE-90 ultracentrifuge using a VTi65.2 rotor. Automated sample fractionation was performed using Lawrence Livermore National Laboratory's high-throughput SIP pipeline, which automates fractionation and clean-up tasks for the density gradient SIP protocol. Ultracentrifuge tube contents were fractionated into 36 fractions (~200 µL each) using an Agilent Technologies 1260 isocratic pump delivering water at 0.25 mL min^{-1} through a 25G needle inserted through the top of the ultracentrifuge tube. Each tube was mounted in a Beckman Coulter fraction recovery system with a side port needle inserted through the bottom. The side port needle was routed to an Agilent 1260 Infinity fraction collector. Fractions were collected in 96-well deep well plates. The density of each fraction was then measured using a Reichart AR200 digital refractometer fitted with a prism covering to facilitate measurement from 5 µL, as previously described[33]. We purified and concentrated DNA in each fraction using a Hamilton Microlab Star liquid handling system programmed to automate previously described glycogen/PEG precipitations[34]. Washed DNA pellets were suspended in 40 µL of 1xTE and the DNA concentration of each fraction was quantified using a PicoGreen fluorescence assay. The fractions for each sample were binned into 9 groups based on density (1.6900-1.7099 g/ml, 1.7100-1.7149 g/ml, 1.7150-1.7199 g/ml, 1.7200-1.7249 g/ml, 1.7250-1.7299 g/ml, 1.7300-1.7349 g/ml, 1.7350-1.7399 g/ml, 1.7400-1.7468 g/ml, 1.7469-1.7720 g/ml), and fractions within a binned group were combined and sequenced.

For 16S rRNA gene amplicon sequencing, non-fractionated DNA as well as density fractionated DNA was amplified in triplicate 10-uL reactions using primers 515 F and 806 R[35,36]. Each reaction contained 1uL sample and 9uL of Phusion Hot Start II High Fidelity master mix (Thermo Fisher Scientific) including 1.5mM additional $MgCl_2$. PCR conditions were 95 C for 2 min followed by 20 cycles of 95 C for 30 S, 64.5 C for 30 S, and 72 C for 1 min. The triplicate

PCR products were then pooled and diluted 10X and used as a template in a subsequent dual indexing reaction that used the same primers including the Illumina flowcell adaptor sequences and 8-nucleotide Golay barcodes (15 cycles identical to initial amplification conditions). Resulting amplicons were purified with AMPure XP magnetic beads (Beckman Coulter) and quantified with a PicoGreen assay on a BioTek Synergy HT plate reader. Samples were pooled at equivalent concentrations, purified with the AMPure XP beads, and quantified using the KAPA Sybr Fast qPCR kit (Kapa Biosciences). A total of 9 unfractionated, and 162 fraction libraries were sequenced on an Illumina MiSeq instrument at Northern Arizona University's Genetics Core Facility using a 300-cycle v2 reagent kit.

Paired-end 151 nt reads were filtered to remove phiX and other contaminants with bbduk v38.56 (default settings except k=31 and hdist=1)[37]. Fastq files were then filtered/trimmed for quality (maxEE=5, truncQ=2) and used to generate amplicon sequence variants (ASVs) with DADA2 v1.10 and phyloseq v1.26[38,39]. Chimeric sequences were determined and removed using removeBimeraDenovo from DADA2. ASV taxonomy was determined using the RDP 16S rRNA gene database (training set 16) using RDP classifier v2.11, keeping classifications with greater than 50% confidence[40]. A phylogenetic tree was built using Muscle v3.8.31 and FastTree v2.1.10[41,42].

Quantitative stable isotope probing analysis

Quantitative stable isotope probing (qSIP) measures the change in buoyant density of a taxon's DNA, or segment of DNA, due to assimilation of a substrate-derived heavy isotope. This shift in buoyant density is measured as the difference in a taxon's weighted average density in a CsCl gradient between the control and isotope addition treatment and is used to estimate the

isotopic enrichment of DNA based on a measured relationship between molecular weight of DNA and isotopic enrichment.

We quantified excess atom fraction (EAF) ^{18}O of bacterial DNA following a modified version of the procedure described by Hungate et al. using average DNA concentration to normalize the relative abundance of taxa within each density fraction[32,43,44] . We calculated median values and 95% confidence intervals for EAF ^{18}O by bootstrapping (n=1000) across experimental replicates. qSIP analysis was limited to taxa that occurred in at least 2 (of 3) experimental replicates and in at least 2 (of 9) density fractions. These criteria were chosen to reduce the likelihood of falsely interpreting spurious density shifts as growth. Technical error associated with tube-level differences in CsCl density gradients was corrected as previously described[45]. When comparing values of ^{18}O enrichment between sites, we used fraction of maximum potential enrichment (FME) ^{18}O to account for small differences in the enrichment of the soil water during incubation. We computed FME ^{18}O for each taxon as EAF ^{18}O divided by enrichment of the soil water.

For all analyses, 'growing' microbial taxa were identified as ASVs having 95% confidence intervals for EAF ^{18}O exceeding zero. We refer to the community of growing microbial taxa at each site as the "growing microbial community". We refer to the microbial community inferred from 16S rRNA marker gene sequencing of non-fractionated DNA at each site as the "total microbial community".

Statistical analyses

All statistical analyses were conducted in R (R Core Team, 2021). Soil properties (total C and N, trace elements, and texture), stable isotopes, and bulk and respired soil radiocarbon values

were compared between sites using one-way ANOVA and Fisher's LSD test. We used one-way ANOVA and Fisher's LSD to test for differences between sites in community and phylum mean FME ^{18}O and only included taxa that were identified as growing at each site in this analysis. We also compared FME ^{18}O of taxa that were growing at Sedgwick only to the FME ^{18}O of taxa that were growing at Sedgwick *and* at least one other site using a t-test. We used linear regression to assess the relationship of taxon-specific FME ^{18}O between sites and included only individual ASVs that were co-occurring in at least two sites.

Phylogenetic signal analyses were used to test whether the growth (EAF ^{18}O) of related organisms resembled each other more than would be expected by chance alone[1]. Phylogeny was built using the SILVA v128 tree using SATé-enabled phylogenetic placement (SEPP)[48,49]. We measured Blomberg's K and Pagel's λ using phytools (Revell, 2012) for taxon-specific EAF ^{18}O values within each site and included all taxa in this analysis.

The relative abundances of taxa in total communities were measured from sequencing of unfractionated DNA samples. The relative abundances of taxa in growing communities were computed by removing counts from taxa that were not identified as growing via qSIP from unfractionated DNA samples and then re-computing relative abundance.

We used Bray-Curtis dissimilarity to assess between-site dissimilarity for both growing and total communities with vegan: Community Ecology Package (Wagner et al. 2019); principal components analysis (PCA) was used to visualize community structure. We tested for differences in community composition between sites using ANOSIM on ranked Bray-Curtis dissimilarities. To test if the degree of community dissimilarity between sites differed for total versus growing microbial communities, we performed a t-test on mean Bray-Curtis dissimilarity for each pairwise comparison of sites between total and growing communities.

Results

Diverging moisture regimes at the grassland sites

Mean annual precipitation decreases and temperature increases between Angelo, the northmost site, and Sedgwick, the southmost site and Hopland experiences rainfall and temperatures intermediate to these two (Table 1). In the calendar year prior to sample collection, the wet season at Angelo and Hopland lasted until April, precipitation remained scarce or absent during the summer months, and returned again by November. In contrast, the wet season at Sedgwick occurred in January and February and didn't return until the following January (Supplementary Figure 1). Total rainfall was above average at Angelo and Sedgwick and below average at Hopland but overall, precipitation and temperature patterns for the year preceding sampling were similar to what we expected based on long-term site level averages; Angelo was the wettest and coldest site and Sedgwick was hottest and driest (Supplementary Table 1). We obtained samples for this study in early 2018 during the wet season when the differences in soil moisture between our sites was minimized. During the 30 days leading up to sample collection, total precipitation differed between our sites by an average of 46 mm and soil moisture upon collection from the field varied only modestly from 17% to 25% (Supplementary Tables 1 & 2).

Soil characterization

Soils at the three grassland sites developed on ancient sedimentary rock, primarily sandstones and shale. At Angelo and Hopland, the wet and intermediate sites, soils are Alfisols and those at Sedgwick, the driest site, are Mollisols indicating intermediate degrees of weathering and soil development at the three sites. Quantitative XRD analysis showed the sites

had a similar composition of minerals with modest variation in their proportions, pointing to shared characteristics of soil parent material and diverging weathering regimes (Supplementary Table 3). Quartz and feldspars dominated the non-clay minerals at all site and clay minerals included kaolinite, chlorite, and muscovite.

In terms of texture, Sedgwick contained the highest proportion of clays (Table 2). This variation in clay content likely contributes to differences in water retention curves, which showed Sedgwick experienced lower soil water potentials at higher moisture contents than the intermediate and wet sites (Supplementary Figure 1). Soil carbon and nitrogen were low at all sites and exhibited little variation. pH decreased with increasing MAP, likely driven by increased leaching of base cations with higher amounts of precipitation[50]. Effective cation exchange capacity and most trace elements were highest in Sedgwick, with the exception of aluminum which was highest in Angelo (Table 2).

	Angelo Avg ± SE	**Hopland Avg ± SE**	**Sedgwick Avg ± SE**	**ANOVA *P***
δ^{13}C Bulk Soil (‰)	-27.54 ± 0.10	-27.64 ± 0.12	-26.99 ± 0.19	**0.04**
δ^{15}N Bulk Soil (‰)	3.75 ± 0.36	4.23 ± 0.28	4.85 ± 0.21	0.10
pH	5.02 ± 0.02	5.55 ± 0.03	6.99 ± 0.03	**<0.0001**
ECEC (meq kg^{-1} soil)	10.99 ± 0.41	10.84 ± 0.39	27.61 ± 0.50	**<0.0001**
% Sand	28 ± 1.53	45 ± 1.16	38 ± 0.88	**<0.0001**
% Silt	42 ± 1.15	36 ± 0.58	28 ± 2.08	**<0.0001**
% Clay	27 ± 0.88	19 ± 1.00	34 ± 0.33	**<0.0001**
% C	1.66 ± 0.31	1.39 ± 0.18	1.99 ± 0.08	0.22

% N	0.13 ± 0.02	0.11 ± 0.01	0.18 ± 0.01	**0.03**
Al (mg kg^{-1})	44.77 ± 1.06	5.17 ± 0.36	*BDL*	**<0.0001**
Ca (mg kg^{-1})	1455.44 ± 52.97	1350.63 ± 47.62	2380.67 ± 50.32	**<0.0001**
K (mg kg^{-1})	98.98 ± 6.34	114.92 ± 13.91	390.39 ± 29.41	**<0.0001**
Mg (mg kg^{-1})	353.39 ± 17.97	448.75 ± 14.92	1760.32 ± 38.34	**<0.0001**
Na (mg kg^{-1})	3.44 ± 1.24	*BDL*	7.21 ± 1.16	**0.03**

Table 2 Soil physical and chemical characteristics of Angelo, Hopland, and Sedgwick (mean ± standard error, n = 3). Differences between grassland means were assessed by one-way ANOVAs and Fisher's LSD. Bold text indicates P-values less than 0.05, and BDL signifies values below detection limit.

Bulk soil and respired $\Delta^{14}C$

The $\Delta^{14}C$ of bulk surface soil increased along the gradient from the wet to the dry site, indicating that the average age of bulk soil C is oldest in the site with the highest annual rainfall (Figure 1). Bulk soil $\Delta^{14}C$ values were above modern at Sedgwick, indicating the presence of carbon associated with atmospheric weapons testing in the 20th century, while the more depleted $\Delta^{14}C$ values observed for soils from Angelo suggest older and more slowly cycling soil C at this site compared to the other sites, and our intermediate Hopland site falls between these two extremes. For reference, turnover times determined using a single-pool, steady-state, homogenous model suggest turnover times of approximately 200, 400, and 700 years for Sedgwick, Hopland, and Angelo, respectively. In contrast, the $\Delta^{14}C$ of respired CO_2 was similar for all soils, and indicated that microorganisms uniformly respired recently fixed C (with an average age of 7 years), despite differences in the average age of bulk soil carbon. The

cumulative effect of diverging precipitation regimes is apparent in bulk soil radiocarbon data, where higher amounts of rainfall appear to support SOM persistence.

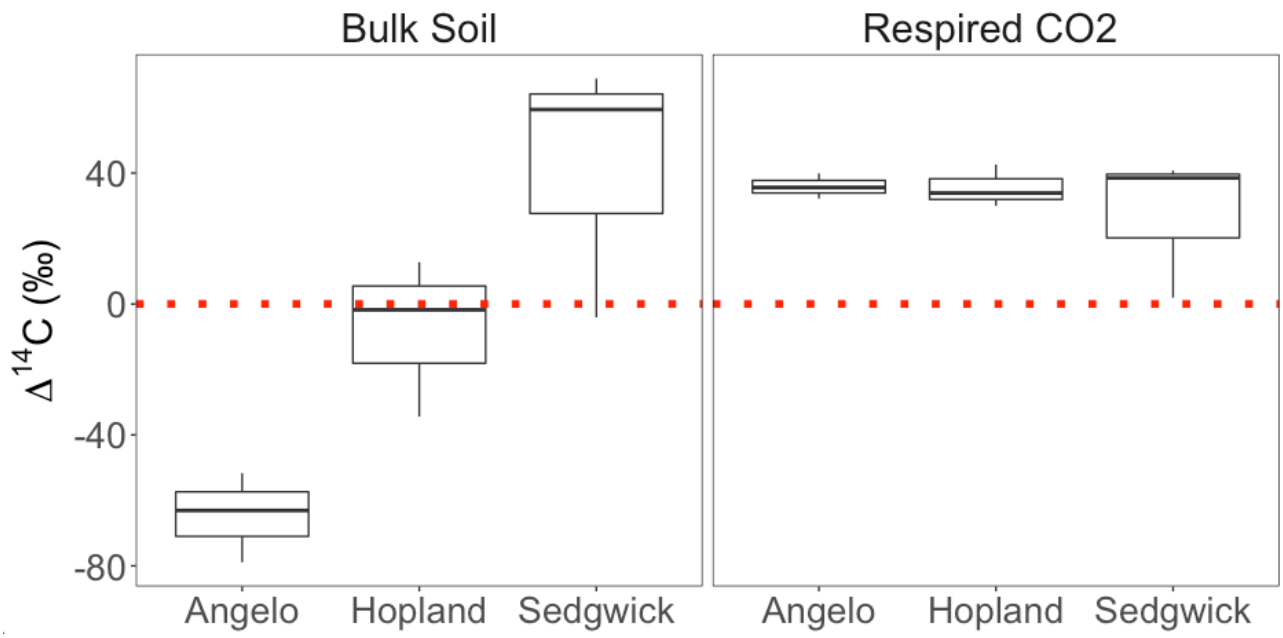

Figure 1 $\Delta^{14}C$ (‰) of bulk soil and respired CO_2. The horizontal line represents atmospheric $\Delta^{14}C$ in 2018 and serves as a reference for post-bomb enrichment. Differences between grassland means were assessed by one-way ANOVAs and Fisher's LSD. $\Delta^{14}C$ (‰) of bulk soils differed between sites ($p<0.05$, Fisher's LSD). $\Delta^{14}C$ (‰) of respired CO2 did not differ between sites ($p>0.05$, Fisher's LSD).

Microbial community structure and growth

Community structure differed by site for both the total and growing bacterial communities (Figure 2). Structure of the total and growing communities at Sedgwick were the most dissimilar from the other sites, as quantified by mean pairwise Bray-Curtis Dissimilarity (Figure 3). Bray-Curtis dissimilarity was statistically indistinguishable between the total and growing microbial communities for each pairwise comparison of community structure between sites Figure 3).

More than 70% of 16S rRNA gene sequences at each site could be attributed to three bacterial phyla: Acidobacteria, Actinobacteria (dominant orders Rubrobacterales, and Solirubrobacterales), and Proteobacteria (dominant orders Burkholderiales, Sphingomonadales, and Rhizobiales). These phyla dominated growing communities as well, comprising more than 80% of all bacterial 16S rRNA gene sequences that were detected by qSIP as growing at each site and accounting for at least 79% of cumulative ^{18}O assimilation in each site (Supplementary Figure 3). While these phyla accounted for a large proportion of total growth, importantly, there was no detectable relationship between the relative abundance of an individual taxon and its growth, meaning low abundance taxa can exhibit fast growth (Supplementary Figure 4).

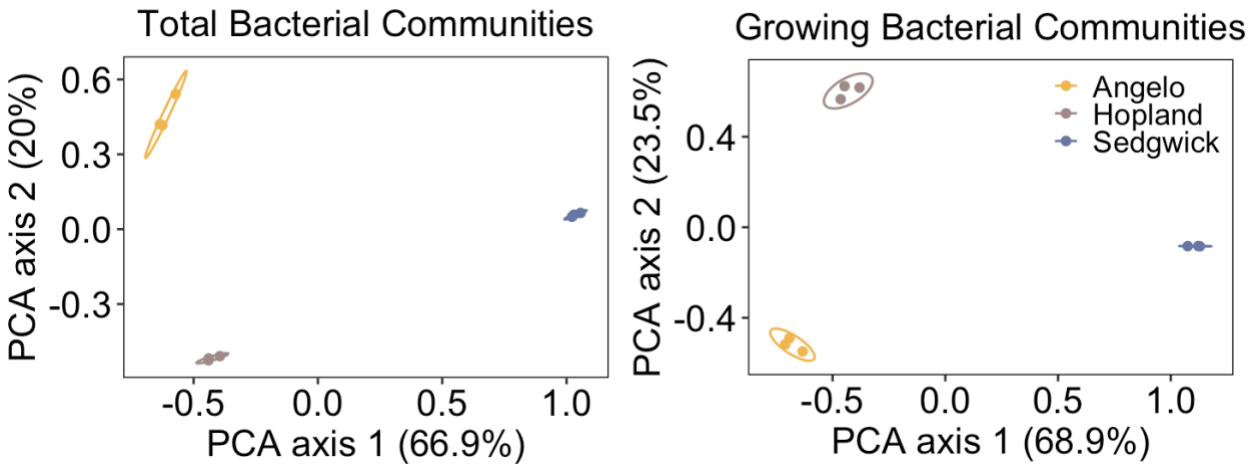

Figure 2 PCoA of Bray-Curtis dissimilarities for total and growing microbial communities. Community composition varies by site for the total microbial communities (ANOSIM, p = 0.0037) and for the growing microbial communities (ANOSIM, p = 0.0027).

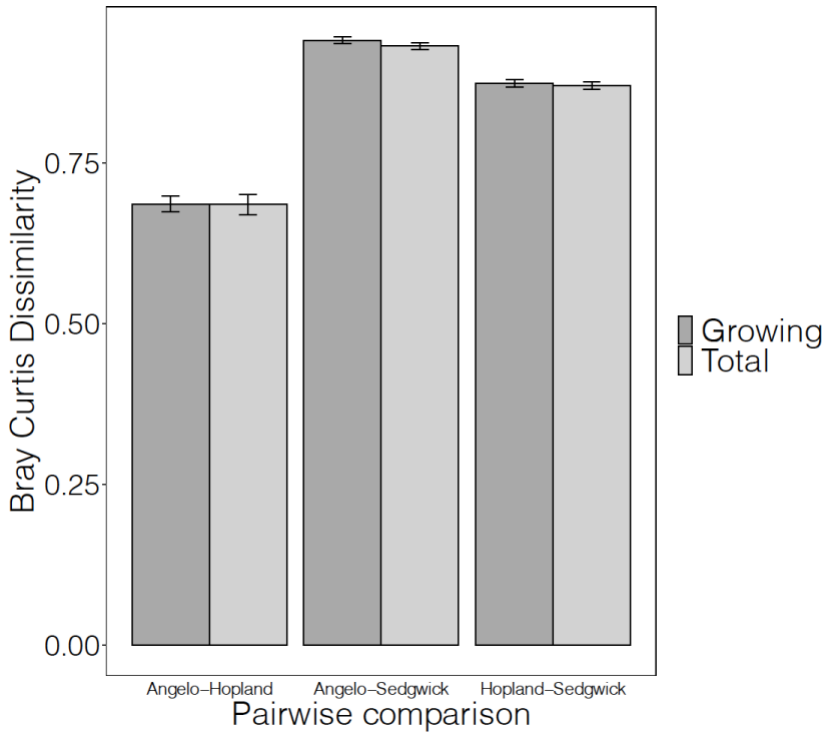

Figure 3 Shows mean pairwise dissimilarity between sites for the present microbial community and growing microbial community. Dissimilarity did not differ for growing versus total communities when comparing between Angelo and Hopland (t-test, $p = 0.95$), Angelo and Sedgwick (t-test, $p = 0.1699$), nor Hopland and Sedgwick(t-test, $p = 0.6453$). Bars show 95% confidence intervals for the means.

Site specific variation in microbial growth was present at the community and phylum levels. Community mean FME ^{18}O was higher in Hopland and Angelo soils than in Sedgwick soils (Figure 4, $p < 0.001$). These patterns, in general, persisted across phyla: Actinobacteria and Bacteroidetes had a higher phylum mean FME ^{18}O in Hopland soils than in Sedgwick soils, and FME ^{18}O was higher in both Angelo and Hopland soils than in Sedgwick soils for the phyla Acidobacteria, Gemmatimonadetes, and Proteobacteria (Figure 4, $p<0.01$). We quantified the percent change in growth for microbial families that were present in Sedgwick and at least one other site and only eight families total (out of 51) exhibited more growth in Sedgwick soils:

Cystobaceraceae, Thermomonosporaceae, Thermoleophilaceae, Rubrobacteraceae, Comamonadaseae, Geminicoccus, Solirubrobacteraceae, and Micromonosporaceae.

For taxa that occurred at more than one site and had detectable growth, their growth rate at one site was predictive of growth rates in another site (Figure 5). We compared ^{18}O enrichment of bacterial ASVs that were present and growing in at least two sites and found positive, linear correlations of taxon-specific enrichment between sites. The growth rate of a bacterial taxon in one site explained as much as 57% of the variation in that taxon's growth rate in another site (Supplementary Table 4). The amount of variation explained by each regression decreases as compositional dissimilarity increased (Supplementary Table 4).

We compared the growth of microorganisms at Sedgwick by grouping taxa according to whether they grew at Sedgwick alone or in at least one other site. We found that taxa that were unique to Sedgwick were slower growing than taxa that were growing in at least one other site (Supplementary Figure 5).

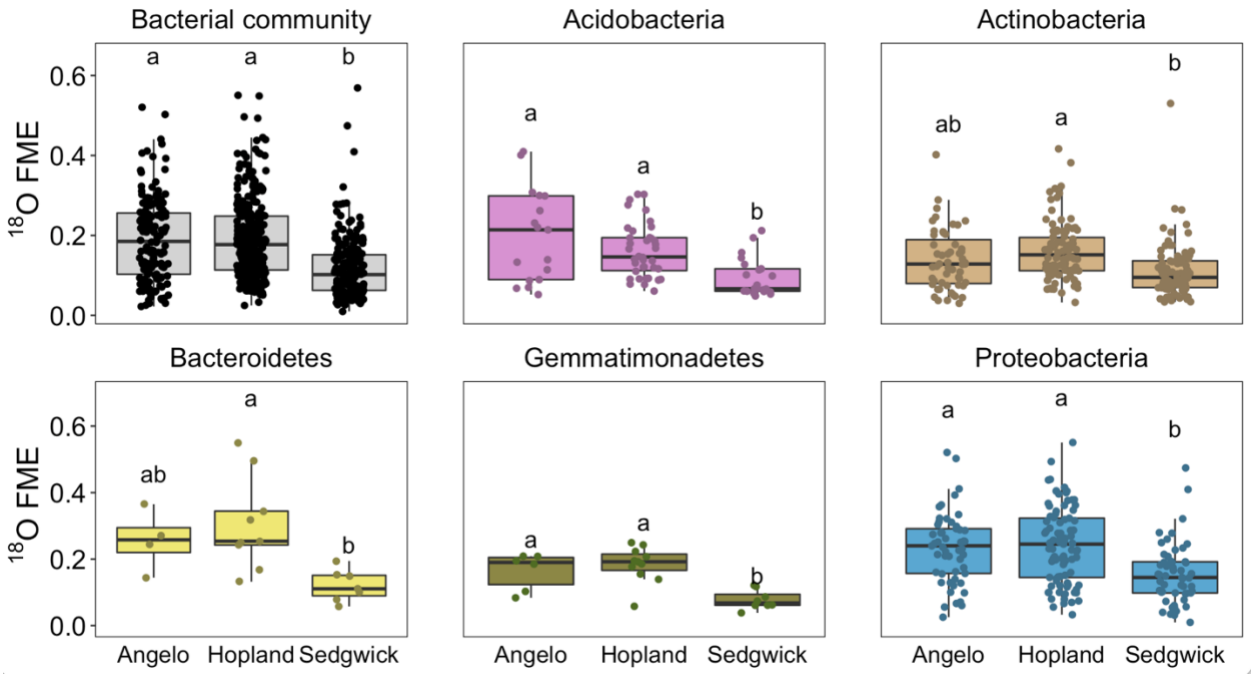

Figure 4 Community and phylum mean FME ^{18}O of microbial taxa that are growing (95% C.I. EAF $^{18}O > 0$) at each grassland site. Letters indicate significant differences between sites ($p<0.05$, Fisher's LSD).

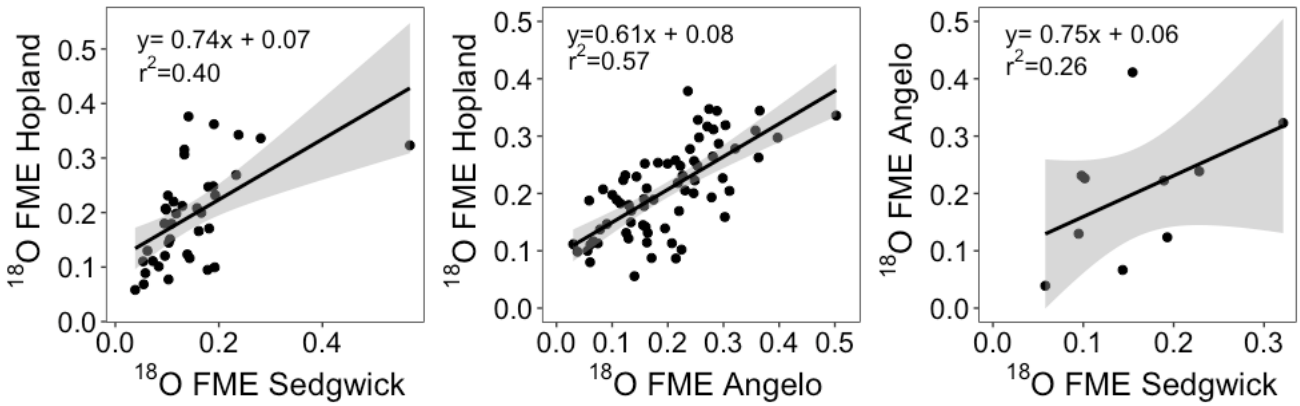

Figure 5 shows linear regressions (black line) of ^{18}O enrichment of microbial taxa co-occuring and in at least two sites. Shaded area shows 95% C.I. for the regression. Regression results are presented in Supplementary Table 4.

We detected significant phylogenetic signals as determined by Pagel's λ and Blomberg's K, for taxon-specific growth (Supplementary Table 5) in all ecosystems. Stronger phylogenetic signals were observed in Angelo ($\lambda = 0.82$, $p<0.001$, $K=0.30$, $p=0.001$) and Hopland ($\lambda = 0.85$, $p<0.001$, $K=0.10$, $p=0.004$) than Sedgwick ($\lambda = 0.68$, $p<0.001$, $K = 0.10$, $p=0.010$). A significant phylogenetic signal indicates that the growth rates of closely related taxa resemble each other more than taxa drawn randomly from the same phylogenetic, however the values we observed are somewhat lower than expected under Brownian motion evolution ($\lambda = 1$ and $K=1$).

Discussion

Structure of growing community mirrors the total community

We hypothesized that the convergence of environmental factors during the weeks preceding sampling would result in growing microbial communities that were compositionally more similar to each other than were total communities. In contrast to this expectation, quantitative measures of between-site dissimilarity were equivalent for growing and total communities (Figure 3). Heavy water quantitative stable isotope probing identifies growing microbial populations (i.e. replicating DNA and synthesizing new biomass), and few studies have compared the structure of growing communities to that of total communities. Some studies have used RNA sequencing to compare the structure of the potentially metabolically active community to that of the total community. These studies have found that potentially active (RNA-based) communities can exhibit distinct biogeographic trends from total microbial communities. For example, an assessment of forested ponds showed that distance decay relationships were stronger for active communities than for total communities[51]. Additionally, a study of arid and semiarid ecosystems found that total communities were more distinct from each other than were active communities[16]. While the results from these studies suggest that mechanisms such as dormancy and relic DNA may influence microbial biogeographic trends at the regional scale, broader evidentiary support in the literature is lacking and the results from our study do not support this finding. Using RNA sequencing to identify metabolically active microbial populations in environmental samples has serious limitations and methodological differences may contribute to the discrepancy between our results and the findings reported in these studies[18]. Instead, our study showed that growing community composition strongly mirrors that of the total community (Supplementary Figure 3).

Persistent Effect of Soil Moisture Limitation on Microbial Growth

We hypothesized that a history of frequent prolonged periods of low soil water potential at the driest site would result in lower microbial growth even when measured under controlled laboratory conditions. Consistent with this expectation, community and phylum mean relative growth rates were higher at the wet and intermediate sites, Hopland and Angelo, than at the driest site, Sedgwick (Figure 4). This variation in growth rate does not appear to be driven by edaphic parameters, as we would expect increasing substrate availability and higher pH levels to, on average, facilitate faster bacterial growth rates[52]. Yet, substrate availability, here best approximated by soil carbon, is highest in Sedgwick soils, the site in which we observed the slowest growth on average. Further, we observed higher growth in the wetter and more acidic soils, Hopland and Angelo.

We hypothesize that in our study, variation in microbial growth reflects a legacy effect of the precipitation regime at the driest site. Similar variation in growth was documented for a precipitation gradient in Texas, where microbial growth decreased with lower MAP when measured under identical conditions in the lab[53]. The literature directly testing the legacy effect of low soil moisture on growth rate is inconsistent. While a number of short-term field and lab experiments have found that historic exposure to drought reduces microbial growth rate, field experiments operating on longer time scales (>10 years) have failed to measure the same effect[8,54–57]. The severity of moisture limitation may impact these findings, as the mentioned long-term experiments featured more mild reductions in rainfall while the short-term experiments featured more intense rainfall reductions.

A number of mechanisms may drive a legacy effect of low soil moisture on microbial growth. Low levels of precipitation could influence growth rates indirectly by altering the quality and quantity of plant carbon inputs during dry periods, reducing the availability of easily-

assimilable substrates later in the year[54]. Slow microbial growth may also be driven by physiological tradeoffs with traits that confer tolerance to water stress. In bacterial isolates, moisture stress has been shown to drive a tradeoff between EPS production and the length of lag phase, suggesting the relevance of growth rate in microbial acclimations to water stress[58].

Such physiological adjustments to low soil water can occur through various mechanisms, including shifts in microbial community composition[9,59]. Our findings suggest that the variability in community and phylum mean growth rates across our sites may influenced by environmental filtering at the driest site for slow-growing taxa that can withstand long periods of low soil water potential. Consistent with current literature, we found evidence for a phylogenetic signal of taxon-specific growth rates[60,61]. Additionally, we found that the growth rate of a bacterial taxon in one site explained as much as 57% of the variation in that taxon's growth rate in another site (Figure 5, Supplementary Table 4), illustrating the relevance of taxonomic identity to growth rate in the environment. Within the community of microorganisms that were growing at the driest site, most (155/197) were found growing at this site alone, and these ASVs that were uniquely growing at Sedgwick demonstrated slower growth, on average, than taxa that occurred and grew in at least one other site (Supplementary Figure 5). So, reduced microbial growth at the driest site appears to be influenced predominantly by relatively slow-growing taxa that are unique to this site. Lastly, the microbial families that actually grew faster in Sedgwick relative to the other sites include taxa that have been described to have traits that would confer an advantage to surviving dry spells. Certain members of the families Cystobacteraceae, Thermomonosporaceae, and Rubrobacteraceae, can form spores[62–64]. The family Comamonadaceae includes the genus variovorax which can accumulate polyhydroxyalkanoates for C storage within the cell and the genome of a species within this same family (genus Ramlibacter) was found to have genes for

carotenoid biosynthesis, EPS synthesis and hydrolysis, and trehalose synthesis[62,65]. We measured microbial growth at the ASV level using qSIP and marker gene sequencing, and we thus lack direct evidence regarding the traits and genomic potential of slow growing taxa at Sedgwick. However future studies combining qSIP with metagenomic sequencing of DNA or RNA would have the potential to reveal such patterns.

Under the conditions evaluated here (wet season, moisture replete soils), the consistent arrangement of growth rates among taxa from site to site (Figure 5), most likely reflects the influence of genetic constraints on growth[60]. This finding suggests that the phenotype of *in situ* growth rate for a given taxon spans a range constrained by its genetics and physiology, constraints that persist across rainfall gradients, edaphic properties, and biological communities. Gradients in climate and edaphic properties are powerful for testing controls over ecosystem processes, including those processes driven by the phenotypes of microorganisms growing in the wild.

Acknowledgements

We thank Erin Nuccio, Amrita Bhattacharyya, Christina Ramon, Aaron Chew, Max Li, and Ryan Gini for assistance with field sampling and lab analyses. We thank John Bailey and Allison Smith at Hopland Research and Extension Center for help gathering meteorological data and the Oregon State University Soil Lab for chemical and physical soil analyses. We would like to thank Thomas Bristow, at the NASA Ames Research Center, for allowing access to his lab space for qXRD analysis. We would like to thank the Mambelli and Dawson Labs at UC Berkeley for stable isotope analysis. This research was supported by the U.S. Department of Energy, Office of Biological and Environmental Research, Genomic Science Program 'Microbes Persist' Scientific Focus Area (#SCW1632) at Lawrence Livermore National Laboratory (LLNL) and a subcontract to Northern Arizona University. Work conducted at LLNL was conducted under the auspices of the US Department of Energy under Contract DE-AC52-07NA27344. Foley MM was supported by a National Science Foundation Graduate Research Fellowship under Grant No. 1938054 while completing this work.

Literature Cited

1. Dore, M. H. I. Climate change and changes in global precipitation patterns: What do we know? *Environ. Int.* **31**, 1167–1181 (2005).
2. Schimel, J. P. Life in Dry Soils: Effects of Drought on Soil Microbial Communities and Processes. *Annu. Rev. Ecol. Evol. Syst.* **49**, 409–432 (2018).
3. Barnard, R. L., Osborne, C. A. & Firestone, M. K. Changing precipitation pattern alters soil microbial community response to wet-up under a Mediterranean-type climate. *ISME J.* **9**, 946–957 (2015).
4. Cruz-Martínez, K. *et al.* Despite strong seasonal responses, soil microbial consortia are more resilient to long-term changes in rainfall than overlying grassland. *ISME J.* **3**, 738–744 (2009).
5. Barnard, R. L., Blazewicz, S. J. & Firestone, M. K. Rewetting of soil: revisiting the origin of soil CO2 emissions. *Soil Biol. Biochem.* 107819 (2020) doi:10.1016/j.soilbio.2020.107819.
6. Hawkes, C. V., Shinada, M. & Kivlin, S. N. Historical climate legacies on soil respiration persist despite extreme changes in rainfall. *Soil Biol. Biochem.* **143**, 107752 (2020).
7. Averill, C., Waring, B. G. & Hawkes, C. V. Historical precipitation predictably alters the shape and magnitude of microbial functional response to soil moisture. *Glob. Change Biol.* **22**, 1957–1964 (2016).
8. Nijs, E. A. de, Hicks, L. C., Leizeaga, A., Tietema, A. & Rousk, J. Soil microbial moisture dependences and responses to drying–rewetting: The legacy of 18 years drought. *Glob. Change Biol.* **25**, 1005–1015 (2019).
9. Evans, S. E. & Wallenstein, M. D. Climate change alters ecological strategies of soil bacteria. *Ecol. Lett.* **17**, 155–164 (2014).

10. Malik, A. A. *et al.* Defining trait-based microbial strategies with consequences for soil carbon cycling under climate change. *ISME J.* **14**, 1–9 (2020).
11. Malik, A. A. *et al.* Drought and plant litter chemistry alter microbial gene expression and metabolite production. *ISME J.* 1–12 (2020) doi:10.1038/s41396-020-0683-6.
12. Flemming, H. C. & Wingender, J. Relevance of microbial extracellular polymeric substances (EPSs)--Part I: Structural and ecological aspects. *Water Sci. Technol. J. Int. Assoc. Water Pollut. Res.* **43**, 1–8 (2001).
13. Sandhya, V. & Ali, Sk. Z. The production of exopolysaccharide by Pseudomonas putida GAP-P45 under various abiotic stress conditions and its role in soil aggregation. *Microbiology* **84**, 512–519 (2015).
14. Maestre, F. T. *et al.* Increasing aridity reduces soil microbial diversity and abundance in global drylands. *Proc. Natl. Acad. Sci.* **112**, 15684–15689 (2015).
15. Angel, R., Soares, M. I. M., Ungar, E. D. & Gillor, O. Biogeography of soil archaea and bacteria along a steep precipitation gradient. *ISME J.* **4**, 553–563 (2010).
16. Angel, R., Pasternak, Z., Soares, M. I. M., Conrad, R. & Gillor, O. Active and total prokaryotic communities in dryland soils. *FEMS Microbiol. Ecol.* **86**, 130–138 (2013).
17. Baubin, C. *et al.* Seasonal and spatial variability in total and active bacterial communities from desert soil. *Pedobiologia* **74**, 7–14 (2019).
18. Blazewicz, S. J., Barnard, R. L., Daly, R. A. & Firestone, M. K. Evaluating rRNA as an indicator of microbial activity in environmental communities: limitations and uses. *ISME J.* **7**, 2061–2068 (2013).

19. Power, M. E., Bouma-Gregson, K., Higgins, P. & Carlson, S. M. The Thirsty Eel: Summer and Winter Flow Thresholds that Tilt the Eel River of Northwestern California from Salmon-Supporting to Cyanobacterially Degraded States. *Copeia* **103**, 200–211 (2015).
20. Sullivan, M. J. P., A.Thomsen, M. & Suttle, K. B. Grassland responses to increased rainfall depend on the timescale of forcing. *Glob. Change Biol.* **22**, 1655–1665 (2016).
21. Dietrich, W. The Problem of Channel Erosion into Bedrock. *undefined* (1992).
22. Berhe, A. A., Suttle, K. B., Burton, S. D. & Banfield, J. F. Contingency in the direction and mechanics of soil organic matter responses to increased rainfall. *Plant Soil* **358**, 371–383 (2012).
23. Fossum, C. *et al.* Belowground allocation and dynamics of recently fixed plant carbon in a California annual grassland soil. *bioRxiv* 2021.08.23.457405 (2021) doi:10.1101/2021.08.23.457405.
24. Homyak, P. M. *et al.* Effects of altered dry season length and plant inputs on soluble soil carbon. *Ecology* **99**, 2348–2362 (2018).
25. Leitner, S. *et al.* Linking NO and N2O emission pulses with the mobilization of mineral and organic N upon rewetting dry soils. *Soil Biol. Biochem.* **115**, 461–466 (2017).
26. Michael Barbour, Todd Keeler-Wolf, & Allan A. Schoenherr. *Terrestrial Vegetation of California, 3rd Edition*. vol. 3rd ed (University of California Press, 2007).
27. Kotanen, P. M. Revegetation following Soil Disturbance and Invasion in a Californian Meadow: a 10-year History of Recovery. *Biol. Invasions* **6**, 245–254 (2004).
28. Minasny, B., McBratney, A. B., Brough, D. M. & Jacquier, D. Models relating soil pH measurements in water and calcium chloride that incorporate electrolyte concentration. *Eur. J. Soil Sci.* **62**, 728–732 (2011).

29. Eberl, D. D. *User Guide to RockJock - A Program for Determining Quantitative Mineralogy from X-Ray Diffraction Data*. http://pubs.er.usgs.gov/publication/ofr200378 (2003) doi:10.3133/ofr200378.

30. Stuiver, M. & Polach, H. A. Discussion Reporting of 14C Data. *Radiocarbon* **19**, 355–363 (1977).

31. Blazewicz, S. J., Schwartz, E. & Firestone, M. K. Growth and death of bacteria and fungi underlie rainfall-induced carbon dioxide pulses from seasonally dried soil. *Ecology* **95**, 1162–1172.

32. Sieradzki, E. T. *et al.* Measurement Error and Resolution in Quantitative Stable Isotope Probing: Implications for Experimental Design. *mSystems* **5**, (2020).

33. Buckley Daniel H., Huangyutitham Varisa, Hsu Shi-Fang, & Nelson Tyrrell A. Stable Isotope Probing with 15N Achieved by Disentangling the Effects of Genome G+C Content and Isotope Enrichment on DNA Density. *Appl. Environ. Microbiol.* **73**, 3189–3195 (2007).

34. Neufeld, J. D. *et al.* DNA stable-isotope probing. *Nat. Protoc.* **2**, 860–866 (2007).

35. Parada, A. E., Needham, D. M. & Fuhrman, J. A. Every base matters: assessing small subunit rRNA primers for marine microbiomes with mock communities, time series and global field samples. *Environ. Microbiol.* **18**, 1403–1414 (2016).

36. Apprill, A., McNally, S., Parsons, R. & Weber, L. Minor revision to V4 region SSU rRNA 806R gene primer greatly increases detection of SAR11 bacterioplankton. *Aquat. Microb. Ecol.* **75**, 129–137 (2015).

37. Bushnell, B. *BBMap: A Fast, Accurate, Splice-Aware Aligner*. https://www.osti.gov/biblio/1241166 (2014).

38. Callahan, B. J. *et al.* DADA2: High-resolution sample inference from Illumina amplicon data. *Nat. Methods* **13**, 581–583 (2016).

39. McMurdie, P. J. & Holmes, S. phyloseq: An R Package for Reproducible Interactive Analysis and Graphics of Microbiome Census Data. *PLOS ONE* **8**, e61217 (2013).

40. Wang, Q., Garrity, G. M., Tiedje, J. M. & Cole, J. R. Naive Bayesian Classifier for Rapid Assignment of rRNA Sequences into the New Bacterial Taxonomy. *Appl. Environ. Microbiol.* **73**, 5261–5267 (2007).

41. MUSCLE: multiple sequence alignment with high accuracy and high throughput | Nucleic Acids Research | Oxford Academic. https://academic.oup.com/nar/article/32/5/1792/2380623 (2020).

42. Price, M. N., Dehal, P. S. & Arkin, A. P. FastTree 2 – Approximately Maximum-Likelihood Trees for Large Alignments. *PLOS ONE* **5**, e9490 (2010).

43. Hungate, B. A. *et al.* Quantitative Microbial Ecology through Stable Isotope Probing. *Appl. Environ. Microbiol.* **81**, 7570 (2015).

44. Papp, K., Hungate, B. A. & Schwartz, E. Microbial rRNA Synthesis and Growth Compared through Quantitative Stable Isotope Probing with $H_2{}^{18}O$. *Appl. Environ. Microbiol.* **84**, e02441-17 (2018).

45. Morrissey, E. M. *et al.* Bacterial carbon use plasticity, phylogenetic diversity and the priming of soil organic matter. *ISME J.* **11**, 1890–1899 (2017).

46. Pagel, M. Inferring the historical patterns of biological evolution. *Nature* **401**, 877–884 (1999).

47. Blomberg, S. P., Garland, T. & Ives, A. R. Testing for Phylogenetic Signal in Comparative Data: Behavioral Traits Are More Labile. *Evolution* **57**, 717–745 (2003).

48. Janssen, S. *et al.* Phylogenetic Placement of Exact Amplicon Sequences Improves Associations with Clinical Information. *mSystems* **3**, e00021-18.

49. Bolyen, E. *et al.* Reproducible, interactive, scalable and extensible microbiome data science using QIIME 2. *Nat. Biotechnol.* **37**, 852–857 (2019).

50. Voroney, R. P. & Heck, R. J. Chapter 2 - The Soil Habitat. in *Soil Microbiology, Ecology and Biochemistry (Fourth Edition)* (ed. Paul, E. A.) 15–39 (Academic Press, 2015). doi:10.1016/B978-0-12-415955-6.00002-5.

51. Locey, K. J. *et al.* Dormancy dampens the microbial distance–decay relationship. *Philos. Trans. R. Soc. B Biol. Sci.* **375**, 20190243 (2020).

52. Rousk, J., Brookes, P. C. & Bååth, E. Contrasting Soil pH Effects on Fungal and Bacterial Growth Suggest Functional Redundancy in Carbon Mineralization. *Appl. Environ. Microbiol.* **75**, 1589–1596 (2009).

53. Leizeaga, A., Hicks, L. C., Manoharan, L., Hawkes, C. V. & Rousk, J. Drought legacy affects microbial community trait distributions related to moisture along a savannah grassland precipitation gradient. *J. Ecol.* **n/a**, (2021).

54. Hicks, L. C., Rahman, M. M., Carnol, M., Verheyen, K. & Rousk, J. The legacy of mixed planting and precipitation reduction treatments on soil microbial activity, biomass and community composition in a young tree plantation. *Soil Biol. Biochem.* **124**, 227–235 (2018).

55. Rahman, M. M., Hicks, L. C., Verheyen, K., Rousk, J. & Carnol, M. Effects of drought legacy and tree species admixing on bacterial growth and respiration in a young forest soil upon drying and rewetting. *Soil Biol. Biochem.* **127**, 148–155 (2018).

56. Meisner, A., Bååth, E. & Rousk, J. Microbial growth responses upon rewetting soil dried for four days or one year. *Soil Biol. Biochem.* **66**, 188–192 (2013).

57. Rousk, J., Smith, A. R. & Jones, D. L. Investigating the long-term legacy of drought and warming on the soil microbial community across five European shrubland ecosystems. *Glob. Change Biol.* **19**, 3872–3884 (2013).

58. Lennon, J. T., Aanderud, Z. T., Lehmkuhl, B. K. & Schoolmaster, D. R. Mapping the niche space of soil microorganisms using taxonomy and traits. *Ecology* **93**, 1867–1879 (2012).

59. Allison, S. D. *et al.* Microbial abundance and composition influence litter decomposition response to environmental change. *Ecology* **94**, 714–725 (2013).

60. Morrissey, E. M. *et al.* Evolutionary history constrains microbial traits across environmental variation. *Nat. Ecol. Evol.* **3**, 1064–1069 (2019).

61. Morrissey, E. M. *et al.* Phylogenetic organization of bacterial activity. *Isme J.* **10**, 2336 (2016).

62. The Family Cystobacteraceae | SpringerLink. https://link.springer.com/referenceworkentry/10.1007%2F978-3-642-39044-9_304.

63. Kroppenstedt, R. M. & Goodfellow, M. The Family Thermomonosporaceae: Actinocorallia, Actinomadura, Spirillospora and Thermomonospora. in *The Prokaryotes: Volume 3: Archaea. Bacteria: Firmicutes, Actinomycetes* (eds. Dworkin, M., Falkow, S., Rosenberg, E., Schleifer, K.-H. & Stackebrandt, E.) 682–724 (Springer, 2006). doi:10.1007/0-387-30743-5_27.

64. Albuquerque, L. & da Costa, M. S. The Family Rubrobacteraceae. in *The Prokaryotes: Actinobacteria* (eds. Rosenberg, E., DeLong, E. F., Lory, S., Stackebrandt, E. & Thompson, F.) 861–866 (Springer, 2014). doi:10.1007/978-3-642-30138-4_202.

65. De Luca, G. *et al.* The Cyst-Dividing Bacterium Ramlibacter tataouinensis TTB310 Genome Reveals a Well-Stocked Toolbox for Adaptation to a Desert Environment. *PLoS ONE* **6**, e23784 (2011).